Available online at www.sciencedirect.com
ScienceDirect
Journal of Colloid and Interface Science 314 (2007) 10–17
JOURNAL OF Colloid and Interface Science
www.elsevier.com/locate/jcis

Ni(II) complexation to amorphous hydrous ferric oxide: An X-ray absorption spectroscopy study

Ying Xu [a], Lisa Axe [b,*], Thipnakarin Boonfueng [b], Trevor A. Tyson [c], Paras Trivedi [d], Kaumudi Pandya [e]

[a] *ConocoPhillips Company, Ponca City, OK 74602, USA*
[b] *Department of Civil and Environmental Engineering, New Jersey Institute of Technology, Newark, NJ 07102, USA*
[c] *Department of Physics, New Jersey Institute of Technology, Newark, NJ 07102, USA*
[d] *Department of Chemistry, Bowdoin College, Brunswick, ME 04011, USA*
[e] *NRL-SRC, National Synchrotron Light Source, Brookhaven National Laboratory, Upton, NY 11026, USA*

Received 12 January 2007; accepted 15 May 2007

Available online 18 May 2007

Abstract

Ni(II) sorption onto iron oxides and in particular hydrous ferric oxide (HFO) is among the important processes impacting its distribution, mobility, and bioavailability in environment. To develop mechanistic models for Ni, extended X-ray absorption fine structure (EXAFS) analysis has been conducted on Ni(II) sorbed to HFO. Coprecipitation revealed the formation of the metastable α-Ni(OH)$_2$ at a Ni(II) loading of 3.5×10^{-3} mol g^{-1}. On the other hand, Ni(II) formed inner-sphere mononuclear bidentate complexes along edges of FeO_6 octahedra when sorbed to HFO surfaces with Ni–O distances of 2.05–2.07 Å and Ni–Fe distances of 3.07–3.11 Å. This surface complex was observed by EXAFS study over 2.8×10^{-3} to 10^{-1} ionic strength, pH from 6 to 7, a Ni(II) loading of 8×10^{-4} to 8.1×10^{-3} mol g^{-1} HFO, and reaction times from 4 hours to 8 months. The short- and long-range structure analyses suggest that the presence of Ni(II) inhibited transformation of the amorphous iron oxide into a more crystalline form. However, Ni^{2+} was not observed to substitute for Fe^{3+} in the oxide structure. This study systematically addresses Ni(II) adsorption mechanisms to amorphous iron oxide. The experimentally defined surface complexes can be used to constrain surface complexation modeling for improved prediction of metal distribution at the iron oxide/aqueous interface.

Keywords: Nickel; Adsorption; Hydrous ferric oxide; Amorphous oxide; EXAFS

1. Introduction

Ni(II) adsorption onto iron oxides and in particular hydrous ferric oxide (HFO) is among the important processes impacting its distribution, mobility, and bioavailability in environment [1–3]. Surface-complexation models (SCM) have proven to be successful in describing metal sorption to mineral surfaces [4]. However, determining the appropriate adsorption mechanisms is critical for successful application of these models over a wide range of conditions [5,6]. Therefore, Ni(II) surface complexes at the HFO–aqueous interface need to be investigated to accurately predict its distribution and bioavailability in soils and sediments.

Although based on an averaged signal, in situ spectroscopic techniques, such as extended X-ray absorption fine structure (EXAFS), are powerful tools among currently available techniques in probing the mineral–aqueous interfaces at a molecular level. EXAFS has been used extensively to determine adsorption mechanisms [7]. Much of the existing Ni EXAFS work has focused on its sorption to aluminum oxides, silica, or related minerals [8–15], where the formation of layered double hydroxide (LDH) precipitates were observed. Elzinga and Sparks [16] reported that adsorption and surface precipitation are consecutive mechanisms involving nonspecific or specific adsorption initially followed by dissolution of Al and nucleation of a mixed Ni/Al phase. The analysis of rates of Ni uptake and Al disso-

* Corresponding author. Fax: +1 (973) 596 5790.
E-mail address: axe@adm.njit.edu (L. Axe).

0021-9797/$ – see front matter
doi:10.1016/j.jcis.2007.05.037

Table 1
Preparation conditions for Ni XAS samples

Sample	pH	IS	Solid ($g\,L^{-1}$)	$[Ni]_0$ (M)	$[Ni]_{eq}$ (M)	Ni_{ads} ($mol\,g^{-1}$)	Reaction time
Ni–HFO-coppt*	7	1.4×10^{-2}	0.2	10^{-2}	9.3×10^{-3}	3.5×10^{-3}	4 h
Ni–HFO-8.1×10^{-3} mol g^{-1} 10^{-3} IS pH 6	6	2.8×10^{-3}	0.1	10^{-2}	9.19×10^{-3}	8.1×10^{-3}	4 h
Ni–HFO-4.0×10^{-3} mol g^{-1} 10^{-2} IS pH 7	7	1.4×10^{-2}	0.2	10^{-2}	9.2×10^{-3}	4.0×10^{-3}	4 h
Ni–HFO-1.0×10^{-3} mol g^{-1} 10^{-2} IS pH 7	7	1.4×10^{-2}	0.5	5×10^{-3}	4.5×10^{-3}	1.0×10^{-3}	4 h
Ni–HFO-3.7×10^{-3} mol g^{-1} 10^{-1} IS pH 7	7	1.0×10^{-1}	0.2	10^{-2}	9.26×10^{-3}	3.7×10^{-3}	4 h
Ni–HFO-5d-8.0×10^{-4} mol g^{-1} 10^{-2} IS pH 7	7	1.4×10^{-2}	1.0	2×10^{-3}	1.2×10^{-3}	8.0×10^{-4}	5 days
Ni–HFO-42d-8.6×10^{-4} mol g^{-1} 10^{-2} IS pH 7	7	1.1×10^{-2}	0.1	10^{-4}	1.4×10^{-5}	8.6×10^{-4}	42 days
Ni–HFO-8m-8.7×10^{-4} mol g^{-1} 10^{-2} IS pH 7	7	1.1×10^{-2}	0.1	10^{-4}	1.3×10^{-5}	8.7×10^{-4}	8 months

* Coppt: coprecipitation.

lution revealed the latter as the rate limiting mechanism [11]. EXAFS studies showed that formation of Ni–Al LDH is characterized by increased second shell contributions as the structure grows [11]. Also, as pH decreased from 7.5 to 6, the rate of formation of LDH precipitates decreased from 15 min to greater than 72 h [13]. Recently, Strathmann and Myneni [17] found that Ni(II) forms inner-sphere mononuclear bidentate complexes with aluminol groups on boehmite (γ-AlOOH), where contact times ranged from 1 to 31 days with loadings between 7.0×10^{-6} and 4.11×10^{-5} mol g^{-1}. The total Ni(II) concentration in their system was about one order of magnitude lower than in other studies where LDH precipitates were observed [10,11,13,14,16,18].

Previous work with Ni sorption to iron oxide has been limited to coprecipitation samples which were aged to promote transformation to hematite and goethite; Ni^{2+} was found to substitute for Fe^{3+} [19–21]. Little has been reported on Ni adsorption to freshly prepared iron oxide surfaces. Although a number of researchers [4,22,23] have modeled adsorption on goethite using SOM^{+} surface species, molecular-scale analyses are needed to corroborate this mechanism. Therefore, the purpose of this work is to investigate the Ni complexation mechanisms on the HFO surface. Both macroscopic and spectroscopic analyses are applied where the effect of pH, ionic strength, loading, and reaction time were investigated. The formation and transformation of HFO in the presence of Ni(II) are also studied.

2. Materials and methods

2.1. Sample preparation

Preparation and characterization of HFO used in this study have been described previously [24–26]. A very broad peak in the X-ray diffractogram was observed and is characteristic of an amorphous structure. Ni(II) adsorption samples were prepared by adding Ni^{2+} (in the form of $Ni(NO_3)_2$ solution) to a freshly prepared HFO suspension under conditions listed in Table 1. The sorption systems were open to the atmosphere to simulate the natural environment. Carbonate species have not been reported to affect adsorption of Zn, Ni, Cd, and Pb under atmospheric conditions [17,27,28]. Moreover, based on the speciation [29], the dominant nickel species is Ni^{2+}. Because BET surface area is measured on freeze-dried particle, it does not necessarily represent that of the hydrous one in the aqueous environment; therefore metal loadings on the hydrated HFO samples were not normalized to the surface area in this study. The bulk aqueous phase Ni(II) concentrations were below the solubility limit for β-$Ni(OH)_2$ (theophrastite) [30,31], which was calculated using MINEQL+ Version 4.5 [32]. Although nickel aqueous speciation and solubility have been reviewed by Hummel and Curti [33] comprehensively, no conclusive thermodynamic data were given therein. Thermodynamic data inherent in MINEQL+ Version 4.5 and compiled by Schecher [34] were used for the solubility and speciation calculations in this work.

All solutions were prepared from Milli-Q Type I DI water. Sodium nitrate was used to adjust ionic strength (10^{-3} to 10^{-1}). Solution pH (6 and 7) was adjusted with 10^{-1} N HNO_3 and NaOH and monitored with pH meter (Accumet model 15), which was calibrated before use. For the Ni–HFO coprecipitation sample, a solution containing both Fe^{3+} and Ni^{2+} (in the form of $Fe(NO_3)_3$ and $Ni(NO_3)_2$, respectively) was prepared and its pH was adjusted to 7–7.5 using 10^{0} and 10^{-1} N NaOH solutions with N_2 purging. The system pH was monitored and adjusted as necessary during the following 4 h of aging. The Ni–HFO-4d and Ni–HFO-8m samples were prepared from constant boundary condition (CBC) experiments conducted in 1 L Nalgene® bottles. The pH and bulk aqueous concentration of metal ion were maintained approximately constant by monitoring and adding 10^{-1} N HNO_3 or NaOH and adsorbate, respectively, as necessary. Turbulence ($Re \geqslant 1.0 \times 10^{4}$) was maintained throughout the studies and centrifugation was used to separate the solid from the aqueous phase. The amount of metal adsorbed was calculated from a mass balance by subtracting final aqueous concentration from initial concentration. Metal

concentrations were analyzed with Beckman Liquid Scintillation System (model LS6500) using an isotope-tagged (Ni^{65}) metal-nitrate stock solution to adjust the concentration. Duplicate samples were prepared: one tagged with Ni^{65} to measure the amount of Ni(II) sorbed, and the other not tagged for EXAFS analyses. Sampling volume was 2 ml. Measurement and adjustment of the concentration were accomplished within several minutes and corrected for volume change to avoid deviation in concentrations between the tagged and untagged samples.

2.2. EXAFS data collection and analysis

The EXAFS data were collected at beamline X-11A at the national synchrotron light source (NSLS), Brookhaven National Laboratory. Data were collected in both transmission and fluorescence modes. The I_0 ion chamber was filled with N_2(g) and the fluorescence signal (I_f) was collected using a Lytle detector filled with Ar gas. The ion chamber for the transmission signal (I_t) was filled with a N_2(g) and Ar(g) mixture adjusted to absorb approximately 60% of the incoming X-rays. EXAFS spectra were collected from 8133 to 8884 eV over the Ni K-edge and from 6912 to 7857 eV over the Fe K-edge. Multiple (about 20–30 for Ni and 5–10 for Fe) scans were averaged to improve signal statistics. The data were analyzed with WinXAS 2.3. Spectra were background corrected and converted to k space following standard procedures [35]. The EXAFS function ($\chi(k)$) was obtained after subtracting the isolated atomic absorption, $\mu_0(E)$, from that in condensed matter. The $\chi(k)$ data were weighted by k^3 to enhance the higher k-space data. Fourier transforms were conducted using the Bessel window function to produce the radial structure function (RSF). Phase shift was not corrected for in the figure but accounted for in fitting with the theoretical model. EXAFS fitting of the RSF was accomplished using theoretical phase shift and amplitude functions calculated with FEFF 7 [36]. Standards for the EXAFS analysis included aqueous Ni^{2+}, $NiCO_3{\cdot}nH_2O$, and NiO.

3. Results and discussion

3.1. Ni–HFO adsorption studies

Preliminary macroscopic studies were conducted to investigate the effect of ionic strength, pH, and Ni concentration. The characteristic sigmoid shape of the adsorption edges (Fig. 1) shows 50% adsorption at about pH 6. The error bars correspond to the standard variation in measuring Ni adsorbed. Consistent with other studies [2,4,37], the effect of ionic strength over 2.8×10^{-3} to 10^{-1} is negligible potentially suggesting that Ni ions form inner-sphere complexes on the HFO surface. A more accurate assessment of adsorption mechanisms over a wider range of conditions is addressed in the following EXAFS study. From isotherms (Fig. 2), the sorbed concentration is linearly related to the bulk aqueous one over a large concentration range (10^{-11}–10^{-3} M), potentially indicative of one average type of adsorption site. This linear relationship was also observed in a study conducted by Trivedi and Axe [38]. To address the coordination environment, EXAFS analysis was conduced.

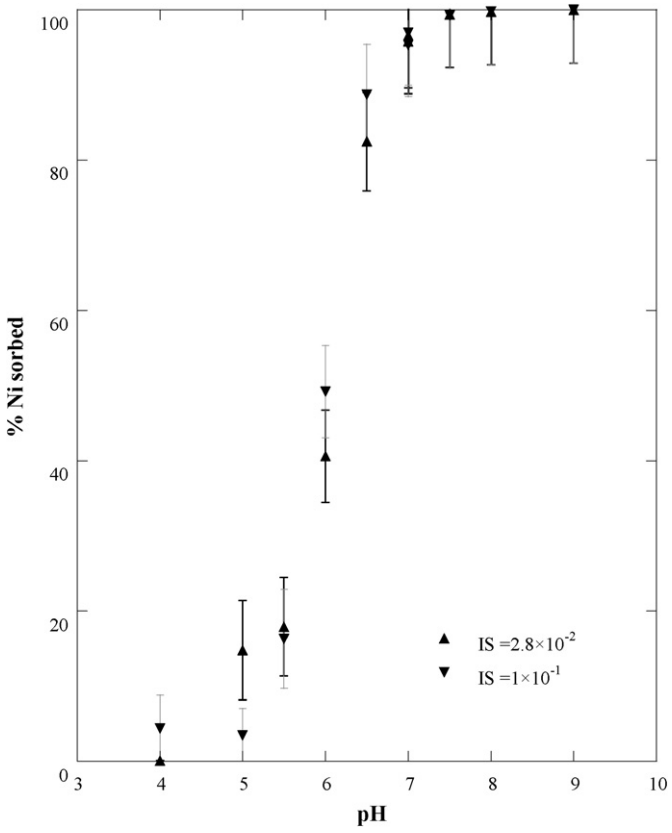

Fig. 1. Ni adsorption edges with 1 g L^{-1} HFO at initial $[Ni]_0 = 5 \times 10^{-9}$ M, $NaNO_3$ based electrolyte, and room temperature.

3.2. EXAFS analysis of Ni

The measurement of EXAFS spectra at energies just greater than the Fe K-edge (i.e. Co, Ni, and Cu) is difficult because the fluorescence signal from trace elements is typically two orders of magnitude less intense (1:100) than the Fe fluorescence from the matrix [19]. To overcome this difficulty, either a high flux X-ray beam or high metal loading is needed. Because the flux at the beamline was fixed, loadings were maximized with initial aqueous concentrations of Ni(II) below its solubility with respect to β-$Ni(OH)_2$ (theophrastite) based on calculations using MINEQL+ Version 4.5 [32] and its inherent thermodynamic database [34]. Additionally, the transmission data were found to have better signal to noise ratio than fluorescence ones and therefore were used in elucidating the Ni local structure.

In the EXAFS analysis of standards (Fig. 3), the $\chi(k) \times k^3$ spectra of aqueous Ni^{2+} ions are dominated by the backscattering from oxygen atoms, resulting in one shell in the FT and consistent with $[Ni(OH_2)_6]^{2+}$ octahedra (Table 2). Richens [39] reported that solutions of $[Ni(OH_2)_6]^{2+}$ are immediately generated upon dissolution of simple Ni^{2+} salts in water containing non- or weakly-coordinating counter-anions. Spectra of the $NiCO_3{\cdot}nH_2O$ and NiO references reveal backscattering from heavier (Ni) atoms (Fig. 3), which represent a second shell in the Fourier transform. For $NiCO_3{\cdot}nH_2O$, the first shell was fit with 6 O atoms at 2.05 ± 0.02 Å and three subshells for the second shell, a carbon shell with 6 atoms at 2.88 ± 0.02 Å, an oxygen shell with 6 atoms at 3.05 ± 0.02 Å, and a Ni shell with

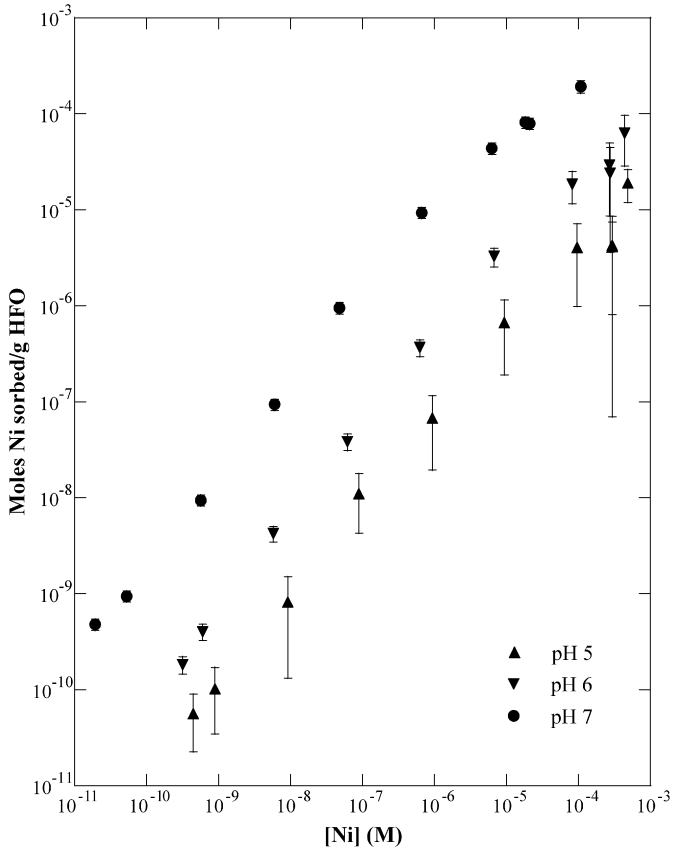

Fig. 2. Ni adsorption isotherms with 1 g L^{-1} HFO as a function of pH at ionic strength 2.8×10^{-2} ($NaNO_3$) and room temperature.

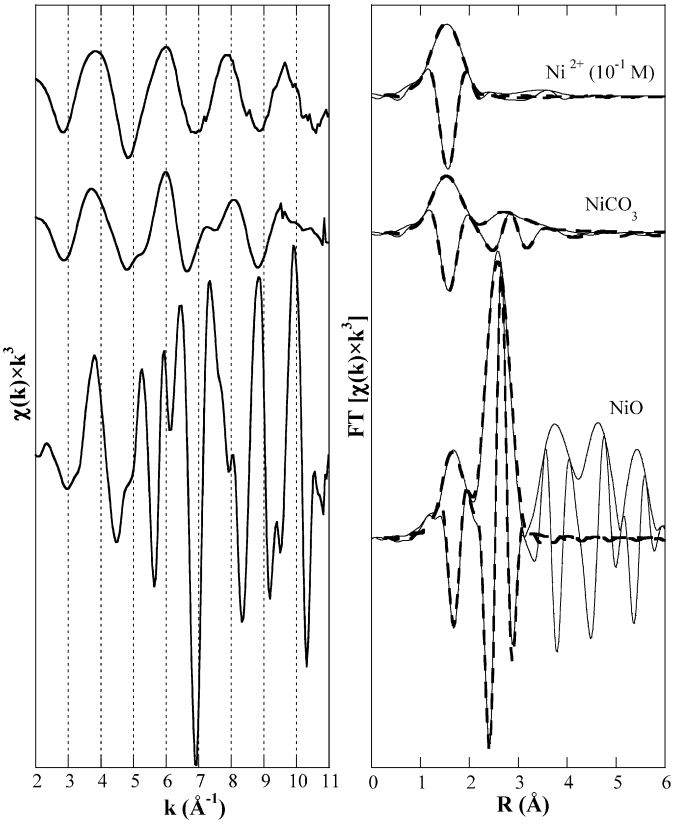

Fig. 3. $\chi(k) \times k^3$ spectra and Fourier transforms (magnitude and imaginary part) of Ni standards at the Ni K-edge at room temperature (Fourier transformed and fitted over ranges: 2.5–10.99 $Å^{-1}$ and 0.73–3.18 Å for NiO; 2.4–9.3 $Å^{-1}$ and 0.65–4.3 Å for $NiCO_3 \cdot nH_2O$; and, 2.36–9.27 $Å^{-1}$ and 0.27–2.23 Å for $Ni^{2+}_{(aq)}$).

6 atoms at 3.53 ± 0.02 Å. The two-shell fitting for NiO resulted in 6 O atoms at 2.07 ± 0.02 Å and 12 Ni atoms at 2.95 ± 0.02 Å. Overall, the above results are consistent with XRD data [40,41].

EXAFS samples (Table 1) included assessing the effect of ionic strength from 2.8×10^{-3} to 10^{-1}, pH 6 to 7, loading from 8×10^{-4} to 8.1×10^{-3} mol Ni g^{-1} HFO, and reaction time from 4 h to 8 months; a coprecipitation sample (3.5×10^{-3} mol Ni g^{-1} HFO) was also prepared for comparison. These spectra (Fig. 4) are unique from that of NiO (Fig. 3) and appear to exhibit a similar envelope as in the Ni^{2+} spectrum (Figs. 3 and 4) except for beat features observed at approximately 5, 7, 8.3, and 9 $Å^{-1}$. The difference suggests backscattering of heavier atoms (Ni or Fe) beyond the first oxygen shell. Although the spectra are somewhat similar to that of $NiCO_3 \cdot nH_2O$ (Figs. 3 and 4), the peak at 6 $Å^{-1}$ shifts slightly to lower k and the shoulder at about 7 $Å^{-1}$ shifts slightly to higher k for the samples. These shifts together with thermodynamic considerations [32], where Ni^{2+} is the dominant species at pH less than 7.7 in an aqueous system open to the atmosphere, suggest $NiCO_3 \cdot nH_2O$ does not precipitate.

The spectrum of Ni–HFO coprecipitation sample however stands out from those of the sorption ones with unique features including a shoulder at about 4.4 $Å^{-1}$ and a discrete peak at 5 $Å^{-1}$ (Fig. 4). This spectrum is identical to that of poorly crystalline hydrated α-$Ni(OH)_2$ obtained by Pandya et al. [42]. Although the most thermodynamically stable form of nickel hydroxide is β-$Ni(OH)_2$ (theophrastite) [30,31], which belongs to the trigonal system with P-3m1 space group [31], the structure of α-$Ni(OH)_2$ is similar to that of β-$Ni(OH)_2$ except that between the (001) planes the presence of water layers results in

Table 2
EXAFS results of Ni standards at Ni K-edge: FT was performed for NiO over 2.50–10.99 $Å^{-1}$, $NiCO_3 \cdot nH_2O$ over 2.4–9.3 $Å^{-1}$, $Ni^{2+}_{(aq)}$ over 2.36–9.27 $Å^{-1}$

Sample	Atom	N	R (Å)	σ^2 ($Å^2$)	ΔE_0 (eV)	Residual
NiO	O	6	2.08			
(XRD result)[a]	Ni	12	2.94			
$NiCO_3$	O	6	2.08			
(XRD result)[b]	C	6	2.93			
	O	6	3.20			
	Ni	6	3.62			
NiO	O	6[c]	2.07	0.01	−3.68	5.55
	Ni	12[c]	2.95	0.01		
$NiCO_3 \cdot nH_2O$	O	6[c]	2.05	0.01	1.64	7.50
	C	6[c]	2.88	0.01		
	O	6[c]	3.05	0.01		
	Ni	6[c]	3.53	0.02		
$Ni^{2+}_{(aq)}$	O	5.9	2.04	0.01	−3.27	4.96

Fits were accomplished over 0.73–3.18 Å for NiO, 0.65–4.3 Å for $NiCO_3 \cdot nH_2O$, and 0.27–2.23 Å for $Ni^{2+}_{(aq)}$. N, coordination number, ±20% error for $Ni^{2+}_{(aq)}$; R, interatomic distance, ±0.02 Å for fitting; σ^2, Debye–Waller factor, ±0.001 $Å^2$; ΔE_0, edge shift.

[a] Wyckoff (1963) [41].
[b] Pertlik (1986) [40].
[c] Fixed during fitting.

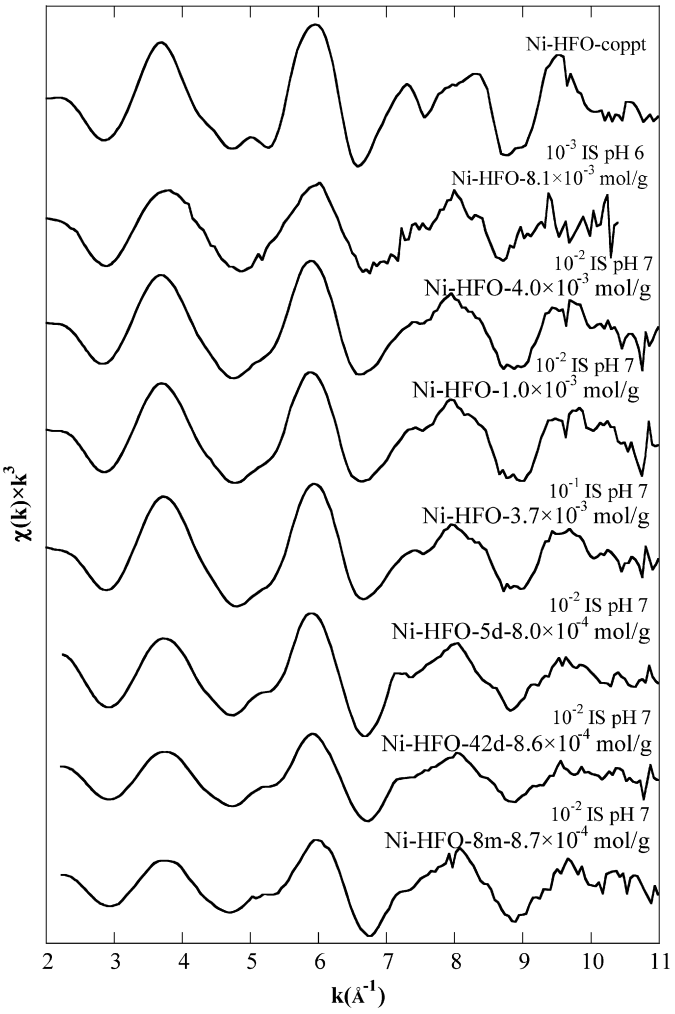

Fig. 4. $\chi(k) \times k^3$ spectra of Ni–HFO sorption complexes as a function of pH, IS, adsorbate loading, and reaction time studied at the Ni K-edge at room temperature.

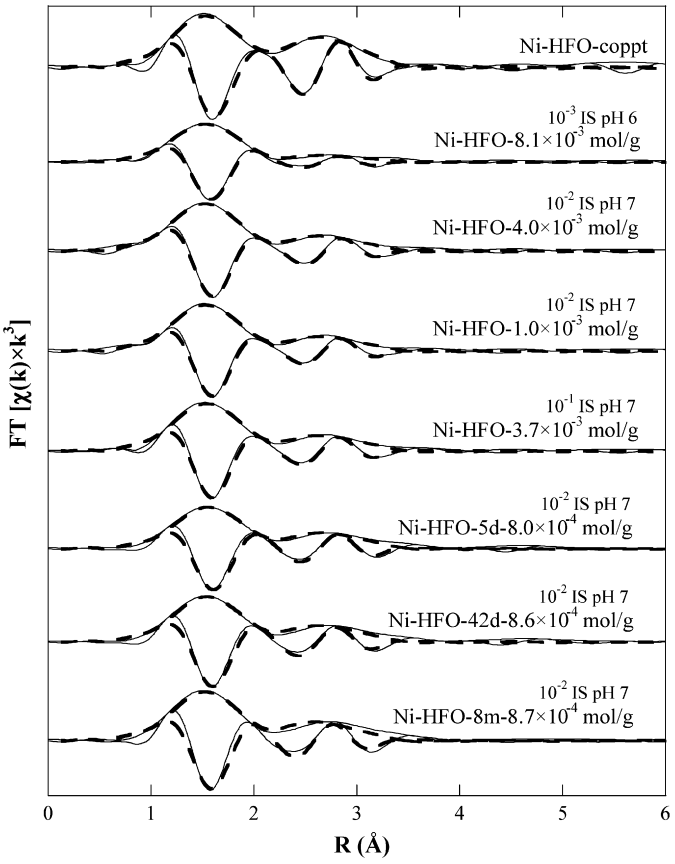

Fig. 5. Fourier transformations (magnitude and imaginary part) of Ni K-edge XAS spectra for Ni–HFO sorption complexes over 2.4–9.3 $Å^{-1}$ and fitted over 0.84–3.80 Å.

an increase in the c-axis spacing [42]. The α-$Ni(OH)_2$ is labile and easily transforms to β-$Ni(OH)_2$ [43]. Therefore metastable α-$Ni(OH)_2$ may have coprecipitated with HFO. The Fourier transform of the $\chi(k) \times k^3$ spectra (Fig. 5) shows a two shell fit with 6.5 O atoms at 2.06 ± 0.02 Å and about 5 Ni atoms at 3.09 ± 0.02 Å (Table 3). Considering the error, fitting results are consistent with that of Pandya et al. [42] where 6 O atoms at 2.04 Å and 5–6 Ni atoms at 3.07 Å were found.

The $\chi(k) \times k^3$ spectra of adsorption samples (Fig. 4) are very similar with one another suggesting similar local structure. The Fourier transforms (Fig. 5) identify two shells; the first shell was fit with 4.8–6.3 O atoms at 2.05–2.07 Å (Table 3) and the second shell could be fit using either Fe or Ni atoms with about the same coordination numbers. Distinguishing between Fe and Ni atoms solely based on EXAFS fitting is difficult, because of the small difference in atomic number, because they have similar ionic radii (0.65 vs 0.69 Å) [39], and because they form similar local structures—octahedral [10,42,44]. However, as the Ni loading increases from 8.0×10^{-4} to 8.1×10^{-3} mol g^{-1}, the number of Ni atoms in the second shell (Table 3) does not increase; these results are not self consistent for polymers or precipitates where the Ni coordination number would increase as the structure grows. Therefore, the second shell is most likely an Fe shell and the formation of a Ni polymer or $Ni(OH)_2$ is ruled out. The differences in $\chi(k) \times k^3$ spectra between the adsorption and coprecipitation samples (Fig. 4) corroborate this conclusion.

With Fe in the second shell, fitting showed 4.8–6.3 of O atoms at 2.05–2.07 Å and 1–2.9 Fe atoms at 3.05–3.11 Å. These results are consistent with two-shell fitting of a coprecipitated Ni–goethite sample [19], where 5.3 O atoms at 2.07 Å and 2.1 Fe atoms at 3.00 Å were obtained. However, two outer shells were also observed by Manceau et al. [19] of 1.4 Fe atoms at 3.18 Å and 2.5 Fe atoms at 3.62 Å, suggesting substitution of Ni^{2+} for Fe^{3+} in the goethite matrix. The absence of multiple Fe shells in our study indicates Ni(II) ions form surface complexes with HFO. Additionally, the Ni–Fe distance of 3.05–3.11 Å suggests formation of bidentate edge-sharing complexes. A more recent study [17] reported similar surface species (mononuclear bidentate edge-sharing surface complexes) for Ni^{2+} sorption on pure boehmite (γ-AlOOH). Fundamentally, aluminum and iron oxides exhibit similar octahedral structural units with comparable Al–O and Fe–O bond lengths [45]; therefore they may have similar surface structures and functional groups. Bargar et al. [45] found Pb(II) surface complexes on iron and aluminum oxides were consistent with one another as well. Therefore, it is not surprising that Ni forms

Table 3
EXAFS results of Ni–HFO samples at Ni K-edge: FT was performed over 2.4–9.3 $Å^{-1}$ in k space and fitted over 0.84–3.8 Å in r space

Sample	Atom	N	R (Å)	σ^2 ($Å^2$)	ΔE_0 (eV)	Residual
Ni–HFO-coppt	O	6.5	2.06	0.01	−4.17	12.89
	Ni	5.0	3.09	0.01		
Ni–HFO-8.1 × 10^{-3} mol g^{-1}	O	4.8	2.05	0.01	−2.69	12.44
10^{-3} IS pH 6	Fe	1.0	3.11	0.01		
Ni–HFO-4.0 × 10^{-3} mol g^{-1}	O	6.0	2.05	0.01	−4.06	8.87
10^{-2} IS pH 7	Fe	2.3	3.11	0.01		
Ni–HFO-1.0 × 10^{-3} mol g^{-1}	O	5.8	2.06	0.01	−3.61	10.58
10^{-2} IS pH 7	Fe	2.3	3.11	0.01		
Ni–HFO-3.7 × 10^{-3} mol g^{-1}	O	6.0	2.06	0.01	−3.02	13.17
10^{-1} IS pH 7	Fe	2.4	3.10	0.01		
Ni–HFO-5d-8.0 × 10^{-4} mol g^{-1}	O	5.5	2.07	0.01	−2.04	13.07
10^{-2} IS pH 7	Fe	2.6	3.11	0.01		
Ni–HFO-42d-8.6 × 10^{-4} mol g^{-1}	O	6.0	2.06	0.01	−2.66	15.22
10^{-2} IS pH 7	Fe	2.6	3.10	0.01		
Ni–HFO-8m-8.7 × 10^{-4} mol g^{-1}	O	6.3	2.05	0.01	−3.08	20.17
10^{-2} IS pH 7	Fe	2.9	3.07	0.01		

N, coordination number, ±20% error; R, interatomic distance, ±0.02 Å; σ^2, Debye–Waller factor, fixed during fitting; ΔE_0, edge shift.

similar surface complexes on iron oxide (this study) and aluminum oxide [17]. Finally, EXAFS spectra reflect an averaged signal and therefore do not depict the full range of site geometries that likely exist [46].

EXAFS results (Table 3, Figs. 4 and 5) suggest that Ni(II) forms inner-sphere mononuclear bidentate complexes along edges of FeO_6 octahedra. This surface complex was observed for ionic strengths 2.8 × 10^{-3} to 10^{-1}, pH 6 to 7, loadings 8 × 10^{-4} to 8.1 × 10^{-3} mol Ni g^{-1} HFO, and reaction times of 4 h to 8 months. Through a constant boundary condition study conducted over 8 days, Trivedi and Axe [38] found as much as 40% of the total sites were located on micropore walls (internal surfaces) of HFO samples; they successfully modeled the sorption data assuming similar internal and external sites. Results of our study further corroborate that sorption to internal and external surfaces potentially involve the same mechanism up to eight months. Because only one Fe shell was observed, Ni^{2+} does not appear to substitute for Fe^{3+}. Under the conditions studied, HFO solubility is approximately three orders of magnitude lower than amorphous aluminum oxide based on MINEQL+ [32]; as a result, LDH formation was not expected.

Previous studies [44,47,48] have shown that HFO exhibits short-range structure and transforms to crystalline forms through progressive long-range ordering. The effect of Ni(II) on the formation and transformation of HFO is addressed in the following section.

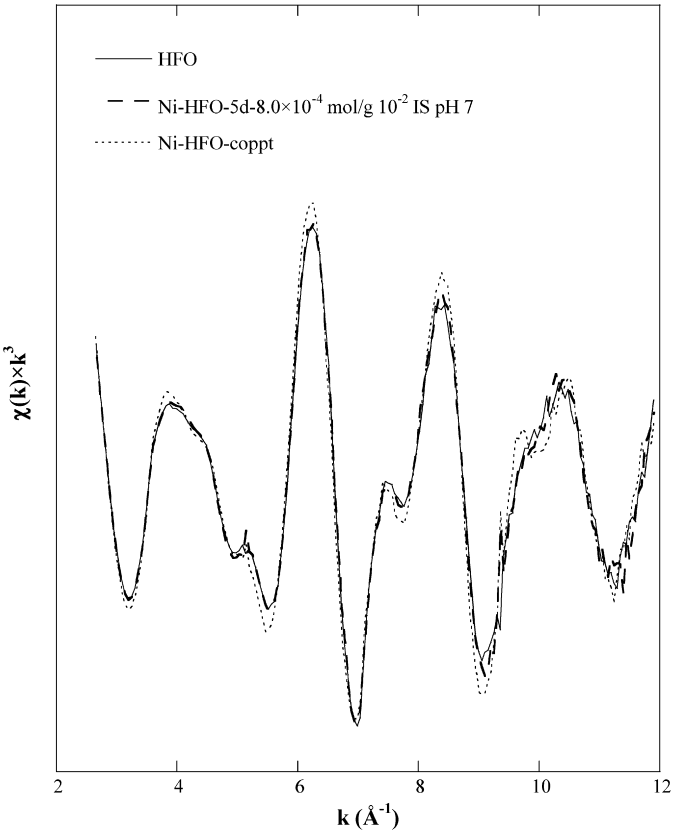

Fig. 6. Fe K-edge $\chi(k) \times k^3$ spectra of HFO, Ni–HFO-5d adsorption sample, and coprecipitated Ni–HFO sample.

3.3. EXAFS analysis of Fe

The $\chi(k) \times k^3$ spectra of discrete HFO, Ni-adsorbed, and Ni-coprecipitated samples (Fig. 6) reveal similar structures. Fitting resulted in (Table 4) 6 O atoms at about 2.03 Å and 2.6–3.6 Fe atoms at 3.07 to 3.09 Å suggesting edge-sharing FeO_6 tetramers. Double corner- or single corner-sharing with Fe–Fe distances longer than 3.29 Å are characteristic of crystalline iron oxides [49] but were not observed. Even at the highest loading of 8.1 × 10^{-3} mol Ni g^{-1}, HFO was still the dominant species based on XRD after aging the sample for 1 year. Similar results have been observed in another study for a Pb–HFO sample after being aged for 21 months [35]. Ni(II) ions bound to surfaces or coprecipitated with HFO may have inhibited crystallization of the amorphous iron oxide.

In studying crystal chemistry and ferrihydrite transformation, synthetic Ni(II) coprecipitated goethite [19,50] and

Table 4
EXAFS results of HFO and Ni–HFO samples at Fe K-edge: FT was performed over 2.86–11.77 $Å^{-1}$ in k space and fitted over 0.52–3.91 Å in r space

Sample	Atom	N	R (Å)	σ^2 ($Å^2$)	ΔE_0 (eV)	Residual
HFO	O	6[a]	2.03	0.01	3.39	24.18
	Fe	3.6	3.08	0.01		
Ni–HFO-5d-8.0 × 10^{-4} mol g^{-1}	O	6[a]	2.03	0.01	2.56	25.55
10^{-2} IS pH 7	Fe	3.0	3.07	0.01		
Ni–HFO-coppt	O	6[a]	2.03	0.01	2.55	22.34
	Fe	2.6	3.09	0.01		

N, coordination number, ±20% error; R, interatomic distance, ±0.02 Å; σ^2, Debye–Waller factor, ±0.001 $Å^2$; ΔE_0, edge shift.
[a] Fixed during fitting.

hematite [20] initially formed as amorphous oxides and were then aged (3, 14, and 93 days, respectively) under elevated temperatures (70–90 °C) and pH (7.5 to ∼13). In another study, Ni^{2+} was coprecipitated with Fe^{3+} at 25 °C, pH > 13, and aged for 16 days [21]. Subsequent EXAFS analysis in all these studies [19–21,50] revealed Ni^{2+} substitution for Fe^{3+}. However, the transformation of HFO to goethite and hematite has been reported to be slow at temperatures below ∼20 °C and is further retarded by adsorbed species [51–55]. In this study, the HFO samples sorbed or coprecipitated with Ni(II) were maintained under room temperature at pH less than or equal to 7. XRD suggests HFO is the dominant iron oxide phase, which did not undergo long-range ordering. Also, considering that Fe atom was not found outside of the second shell of Ni, these observations may suggest that Ni^{2+} did not substitute for Fe^{3+}. The substitution requires crystal growth of iron oxides where Ni octahedra would have been buried into the Fe octahedral network.

4. Summary

Ni(II) adsorption on HFO samples has been studied with EXAFS. Results suggest that Ni(II) forms mononuclear bidentate edge-sharing surface complexes upon adsorption to HFO. This mechanism did not change as a function of ionic strength 2.8×10^{-3} to 10^{-1}, pH 6–7, loading 8×10^{-4} to 8.1×10^{-3} mol Ni g^{-1} HFO, and reaction time 4 h to 8 months. The presence of Ni(II) potentially inhibited HFO transformation into a more crystalline iron oxide; therefore the large sorption capacity of HFO was maintained throughout the adsorption studies. Ni^{2+} was not found to substitute for Fe^{3+} up to 8 months at room temperature, possibly because HFO did not undergo phase transformation into a more crystalline form. Metastable α-$Ni(OH)_2$ appears to have formed when coprecipitated with HFO. This study is among the first in systematically addressing Ni(II) adsorption mechanisms to amorphous iron oxide. The experimentally defined surface complexes can be used to constrain surface complexation modeling as recently applied [46] for improved description and prediction of Ni distribution at the iron oxide/aqueous interfaces.

Acknowledgments

This material is based upon work supported by the DuPont Young Professor's Grant and the National Science Foundation under Grant No. BES 0089903. The authors thank James A. Dyer and Noel C. Scrivner of DuPont Engineering Technology for their input and support. We appreciate the technical support provided by staff at beamline X11A and X11B, National Synchrotron Light Source (NSLS), Brookhaven National Laboratory (BNL). Research carried out at NSLS BNL is supported in part by the US Department of Energy, Division of Materials Sciences and Division of Chemical Sciences, under Contract DE-AC02-98CH10886.

References

[1] R.G. Ford, P.M. Bertsch, K.J. Farley, Environ. Sci. Technol. 31 (1997) 2028–2033.
[2] H. Green-Pedersen, B.T. Jensen, N. Pind, Environ. Technol. 18 (1997) 807–815.
[3] H. Green-Pederson, N. Pind, Colloids Surf. A 168 (2000) 133–145.
[4] D.A. Dzombak, F.M.M. Morel, Surface Complexation Modeling: Hydrous Ferric Oxide, Wiley, New York, 1990.
[5] L.E. Katz, K.F. Hayes, J. Colloid Interface Sci. 170 (1995) 491–501.
[6] J.A. Dyer, P. Trivedi, N.C. Scrivner, D.L. Sparks, Environ. Sci. Technol. 37 (2003) 915–922.
[7] G.E. Brown Jr., N.C. Sturchio, An overview of synchrotron radiation applications to low temperature geochemistry and environmental science, in: P.A. Fenter, N.C. Rivers, S.R. Sturchio, S.R. Sutton (Eds.), Applications of Synchrotron Radiation in Low-Temperature Geochemistry and Environmental Science, in: Rev. Mineral. Geochem., vol. 49, Mineralogical Society of America, Washington, DC, 2002, pp. 1–115.
[8] O. Clause, M. Kermarec, L. Bonneviot, R. Villain, M. Che, J. Am. Chem. Soc. 114 (1992) 4709–4717.
[9] J.L. Paulhiac, O. Clause, J. Am. Chem. Soc. 115 (1993) 11602–11603.
[10] A.M. Scheidegger, G.M. Lamble, D.L. Sparks, Environ. Sci. Technol. 30 (1996) 548–554.
[11] A.M. Scheidegger, D.G. Strawn, G.M. Lamble, D.L. Sparks, Geochim. Cosmochim. Acta 62 (1998) 2233–2245.
[12] R.G. Ford, A.C. Scheinost, K.G. Scheckel, D.L. Sparks, Environ. Sci. Technol. 33 (1999) 3140–3144.
[13] D.R. Roberts, A.M. Scheidegger, D.L. Sparks, Environ. Sci. Technol. 33 (1999) 3749–3754.
[14] M. Nachtegaal, D.L. Sparks, Environ. Sci. Technol. 37 (2003) 529–534.
[15] A. Voegelin, R. Kretzschmar, Environ. Sci. Technol. 39 (2005) 5311–5318.
[16] E.J. Elzinga, D.L. Sparks, J. Colloid Interface Sci. 213 (1999) 506–512.
[17] T.J. Strathmann, S.C.B. Myneni, Environ. Sci. Technol. 39 (2005) 4027–4034.
[18] A.C. Scheinost, R.G. Ford, D.L. Sparks, Geochim. Cosmochim. Acta 63 (1999) 3193–3203.
[19] A. Manceau, M.L. Schlegel, M. Musso, V.A. Sole, C. Gauthier, P.E. Petit, F. Trolard, Geochim. Cosmochim. Acta 64 (2000) 3643–3661.
[20] B. Singh, D.M. Sherman, R.J. Gilkes, M. Wells, J.F.W. Mosselmans, Clays Clay Miner. 48 (2000) 521–527.
[21] B. Singh, D.M. Sherman, R.J. Gilkes, M.A. Wells, J.F.W. Mosselmans, Clay Miner. 37 (2002) 639–649.
[22] B.R. Coughlin, A.T. Stone, Environ. Sci. Technol. 29 (1995) 2445–2455.
[23] D. Buerge-Weirich, R. Hari, H. Xue, P. Behra, L. Sigg, Environ. Sci. Technol. 36 (2002) 328–336.
[24] D.A. Dzombak, F.M.M. Morel, J. Colloid Interface Sci. 112 (1986) 588–598.
[25] L. Axe, P.R. Anderson, J. Colloid Interface Sci. 175 (1995) 157–165.
[26] P. Trivedi, L. Axe, J. Colloid Interface Sci. 218 (1999) 554–563.
[27] L.S. Balistrieri, J.W. Murray, Geochim. Cosmochim. Acta 46 (1982) 1253–1265.

[28] P. Trivedi, L. Axe, T.A. Tyson, J. Colloid Interface Sci. 244 (2001) 230–238.
[29] Y. Xu, Heavy metal adsorption on iron oxide and iron oxide-coated silica: Macroscopic, spectroscopic, and modeling studies, Ph.D. dissertation, Department of Civil and Environmental Engineering, New Jersey Institute of Technology, Newark, NJ, October 2005.
[30] C.F. Baes Jr., R.E. Mesmer, The Hydrolysis of Cations, Wiley, 1976.
[31] H. Wallner, K. Gatterer, Z. Anorg. Allg. Chem. 628 (2002) 2818–2820.
[32] MINEQL+ Version 4.5: Equilibrium Modeling System. Environmental Research Software, 1998.
[33] W. Hummel, E. Curti, Monatsh. Chem. 134 (2003) 941–973.
[34] W. Schecher, Thermochemical Data Used in MINEQL+ version 4.5, Environmental Research Software, 2001.
[35] Y. Xu, T. Boonfueng, L. Axe, S. Maeng, T. Tyson, J. Colloid Interface Sci. 299 (2006) 28–40.
[36] S.I. Zabinsky, J.J. Rehr, A. Ankudinov, R.C. Albers, M.J. Eller, J. Phys. Rev. B Condens. Matter 52 (1995) 2995–3009.
[37] K.F. Hayes, J.O. Leckie, J. Colloid Interface Sci. 115 (1987) 564–572.
[38] P. Trivedi, L. Axe, J. Colloid Interface Sci. 244 (2001) 221–229.
[39] D.T. Richens, The Chemistry of Aqua Ions, Wiley, Chichester, UK, 1997.
[40] F. Pertlik, Acta Crystallogr. C 42 (1986) 4–5.
[41] R.W.G. Wyckoff, Crystal Structure, vol. 1, III, Interscience Publishers, New York, 1963.
[42] K.I. Pandya, W.E. O'Grady, D.A. Corrigan, J. McBreen, R.W. Hoffman, J. Phys. Chem. 94 (1990) 21–26.
[43] H. Bode, K. Dehmelt, J. Witte, Electrochim. Acta 11 (1966) 1079–1087.
[44] J.M. Combes, A. Manceau, G. Calas, J.Y. Bottero, Geochim. Cosmochim. Acta 53 (1989) 583–594.
[45] J.R. Bargar, G.E. Brown Jr., G.A. Parks, Geochim. Cosmochim. Acta 61 (1997) 2639–2652.
[46] Y. Xu, L. Axe, N. Yee, J.A. Dyer, Environ. Sci. Technol. 40 (2006) 2213–2218.
[47] J.M. Combes, A. Manceau, G. Calas, Geochim. Cosmochim. Acta 54 (1990) 1083–1091.
[48] A. Manceau, V. Drits, Clay Miner. 28 (1993) 165–184.
[49] L. Charlet, A.A. Manceau, J. Colloid Interface Sci. 148 (1992) 443–458.
[50] M.L. Carvalho-E-Silva, A.Y. Ramos, H.C.N. Tolentino, J. Enzweiler, S.M. Netto, M.D.C.M. Alves, Am. Mineral. 88 (1992) 876–882.
[51] U. Schwertmann, H. Thalmann, Clay Miner. 11 (1976) 189–200.
[52] R.M. Cornell, R. Giovanoli, P.W. Schindler, Clays Clay Miner. 35 (1987) 21–28.
[53] R.M. Cornell, R. Giovanoli, Polyhedron 7 (1988) 385–391.
[54] C.R. Paige, W.J. Snodgrass, R.V. Nicholson, J.M. Scharer, Q.H. He, Water Air Soil Pollut. 97 (1997) 397–412.
[55] C.E. Martínez, M.B. McBride, Clays Clay Miner. 46 (1998) 537–545.